Which transition metal atoms can be embedded into two-dimensional molybdenum dichalcogenides and add magnetism?

Which transition metal atoms can be embedded into two-dimensional molybdenum dichalcogenides and add magnetism?

J. Karthikeyan,[†] Hannu-Pekka Komsa,[†] Matthias Batzill,[‡] and Arkady V. Krasheninnikov[*,¶,†]

†Department of Applied Physics, Aalto University, P.O. Box 11100, 00076 Aalto, Finland

‡Department of Physics, University of South Florida, Tampa, Florida 33620, United States

¶Institute of Ion Beam Physics and Materials Research, Helmholtz-Zentrum Dresden-Rossendorf, 01328 Dresden, Germany

E-mail: karthikeyan.jeyakumar@aalto.fi;a.krasheninnikov@hzdr.de

Abstract

As compared to bulk solids, large surface-to-volume ratio of two-dimensional (2D) materials may open new opportunities for post-synthesis introduction of impurities into these systems by, e.g., vapor deposition. However, it does not work for graphene or h-BN, as the dopant atoms prefer clustering on the surface of the material instead of getting integrated into the atomic network. Using extensive first-principles calculations, we show that counterintuitively most transition metal (TM) atoms can be embedded into the atomic network of the pristine molybdenum dichalcogenides (MoDCs) upon atom deposition at moderate temperatures either as interstitials or substitutional impurities, especially in $MoTe_2$, which has the largest spacing between the host atoms. We further demonstrate that many impurity configurations have localized magnetic

1

moments. By analyzing the trends in energetics and values of the magnetic moments across the periodic table, we rationalize the results through the values of TM atomic radii and the number of $(s + d)$ electrons available for bonding, and suggest the most promising TMs for inducing magnetism in MoDCs. Our results are in line with the available experimental data and should further guide the experimental effort towards a simple post-synthesis doping of 2D MoDCs and adding new functionalities to these materials.

Keywords: two-dimensional materials, transition metal dichalcogenides, doping, impurities, electronic structure calculations, magnetism.

Impurities in solids, especially semiconductors, frequently govern their properties, so that nowadays doping is a standard way to tailor materials characteristics and add new functionalities. The dopants can naturally be present in the solid or deliberately introduced by ion implantation.[1] In synthetic materials, impurities can also be added during their growth.[2] Both doping methods work for two-dimensional (2D) systems. For example, nitrogen or boron atoms can be embedded into carbon network during the growth of graphene[3–5] or by low-energy ion implantation.[6–9] Likewise, impurities can be introduced into transition metal dichalcogenides (TMDs), another class of 2D materials with diverse properties,[10–13] during growth[14–17] or by irradiation.[18,19]

However, as compared to the bulk systems, there is another way to dope 2D materials: as they consist of essentially the surface only, impurities can be added by simply depositing the dopant atoms after the reactivity of the system has been enhanced by creating defects using electron[15,20] or ion[19] irradiation, or plasma treatment.[21,22] Moreover, for some pristine 2D materials, e.g. $MoTe_2$, but not graphene or h-BN, deposition of transition metal (TM) atoms at elevated temperatures has been demonstrated to give rise to the direct incorporation of the atoms into the atomic network. Specifically, the incorporation of Mo has been reported[23] to cause restructuring of the crystal and developing metal-rich mirror-twin-boundaries (MTBs) in $MoSe_2$ and $MoTe_2$, which may open new avenues for tailoring the electronic and catalytic properties of the material. Post-synthesis doping of $MoTe_2$ with V and Ti atoms using that same technique has also been shown.[24] A room-temperature ferromagnetic semiconductor was manufactured by incorporation of V atoms into the atomic network of $MoTe_2$. The material was found to be stable in air, and its magnetic properties could further be tuned by high-temperature annealing. At the same time, doping with Ti instead of V did not result in magnetism in spite of a similar incorporation behavior.[24] Magnetism in Mn-doped MoS_2 has been reported as well.[25]

This gives rise to several questions, which should be important in the context of both fundamental physics of defects in low-dimensional systems and practical engineering of the

electronic and magnetic properties of 2D TMDs by metal deposition, such as: (*i*) Which TM atoms can be incorporated into the atomic network of TMDs? (*ii*) If incorporation is possible, which atomic configurations will be stable? (*iii*) What would be the electronic and magnetic properties of the doped TMDs? Although there are reports[26] on the electronic and magnetic properties of TMDs and specifically MoS_2 with Re,[14,27] Nb[28] and magnetic (Fe, Co, etc.) TM atoms[29,30] in substitutional,[29,31] interstitial[30] and adatom positions,[32,33] as well as at the edges of the platelets,[34] there are no theoretical studies which would systematically address the above questions, while the first experimental results[24] indicate that post-synthesis doping of TMDs by deposition of TMs is a very promising technique to add magnetism to TMDs. Here we carry out extensive first-principles calculations for essentially *all* TMs and analyze the stability of various impurity configurations. We concentrate on hexagonal molybdenum dichalcogenides (MoDCs = MoS_2, $MoSe_2$ and $MoTe_2$) and pay particular attention to the magnetic properties of the system.

We aim at mimicking the experimental deposition of TM atoms, wherein the deposited atoms first land on the surface as adatoms, then diffuse, and finally either agglomerate into TM clusters or get absorbed inside the MoDC sheet, as illustrated in Fig. 1. To this end, we first studied the adsorption of TM atoms on MoDCs, starting the atomic relaxation with the high-symmetry positions of adatoms. We found that there are two stable adatom positions: the TM atom can be adsorbed on top of the middle of the hexagon (hollow or "h-Top" position) or on top of the Mo site ("Mo-Top") as shown in Fig. 1. The position on top of the chalcogen atom was either unstable or much higher in energy. To understand if their incorporation into the atomic network is energetically favorable, as compared to their agglomeration on the surface, we calculated several other sites for the TM atoms, such as interstitial ("Int") or chalcogen (X) site with the chalcogen atom displaced to adatom site "X-Sub", cf. Fig. 1). For some TMs in the "X-Sub" configuration, the TM atom could also be displaced towards the hollow site, as illustrated in Fig. S1. All these configurations have the same stoichiometry, as expected upon deposition on pristine MoDCs, and thus allow for
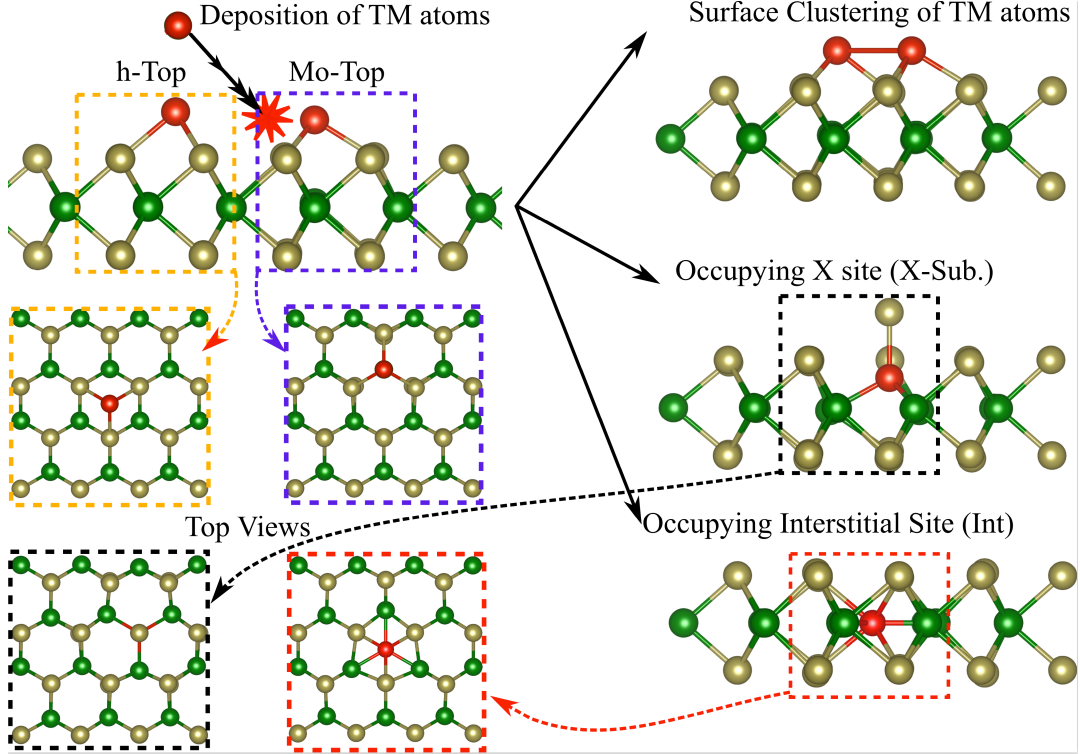
Figure 1: Schematic representation of transition metal (TM) atom deposition on MoDC layers and the atomic structures of TM adatoms and atoms embedded into MoDC. After deposition the TM adatoms can agglomerate and form dimers as well as larger clusters, or be incorporated into the atomic network in the interstitial site or substituting for the chalcogen atom X=S/Se/Te. The green, ochre, and red balls represent host Mo, chalcogen, and TM atoms, respectively.

direct comparison of formation energies.

In order to get insight into the atomic structure, stability and properties of MoDCs doped with TM atoms, we carried out first-principles calculations for the 6×6×1 supercells of MoDCs with single TM atom aiming at the low-concentration limit of impurities. We used the density functional theory (DFT) as implemented in the VASP code,[35,36] with the PBE exchange and correlation functional.[37] The Brillouin zone of the supercell was sampled with a 3×3×1 k-mesh. We did not account for onsite Coulomb interaction, as the choice of the corresponding Hubbard term U is somewhat arbitrary, and normally the optimum value of U for a specific compound is chosen to match the reference data, while we wanted to assess general trends in energetics and magnetism of TM atoms in MoDCs across the periodic

table. Our simulation setup is expected to give at least qualitatively correct description of the energetics and the electronic structure of impurities, although for some TMs a more accurate account for correlations and spin-orbit coupling may give rise to changes in the local magnetic moments.

Having optimized the geometry, we calculated the formation energies E_f of these configurations as $E_f = E(\mathrm{L} + \mathrm{TM}) - E(\mathrm{L}) - \mu_{\mathrm{TM}}$, where $E(\mathrm{L} + \mathrm{TM})$ and $E(\mathrm{L})$ are the total energies of the supercell with the TM and pristine MoDC layer, and μ_{TM} is the Chem. potential of the TM atom in the isolated TM dimer defined as $\mu_{\mathrm{TM}} = \frac{1}{2}E(\mathrm{dimer})$. We chose the dimer as a reference system to represent the first step in the adatom agglomeration. Essentially, we assume that the deposition rate is rather low, and at the same time, the temperature is high enough to facilitate incorporation of TM atoms into the atomic network of MoDCs if it is energetically favorable, so that quick formation of metal clusters is unlikely. In any case, all the energies can trivially be rescaled if a different reference system (e.g., bulk metal or isolated atom) is chosen as a reference, or the interaction of the dimer with the surface (0.2 - 0.7 eV) is taken into account. The trends, however, will remain the same. All the energies are also listed in Tables T1-T6 in supporting information.

E_f for all TMs in the adatom ("Mo-Top" and "h-Top") positions is presented in Fig. 2, along with energies for interstitial ("Int") and substitutional chalcogen atom site ("X-Sub") configurations. The data indicates that in MoS_2, E_f is higher for interstitials than for adatoms or substitutional configurations, which means that most TM adatoms will stay on the surface and likely form clusters. This is in agreement with the experimental reports: the attempts to dope MoS_2 with e.g. Co or Au have proven to be unsuccessful, and the atoms remained either at adatom sites or at flake edges.[14,38] Mn impurities in MoS_2 were reported[39] to be predominantly at domain boundaries, although substitutional impurities were also present.

The same is true for $4d$ and $5d$ TMs in $MoSe_2$, while for many of the $3d$ TMs all three configurations are competitive. For all MoDCs, the late TMs (zinc and copper, and perhaps
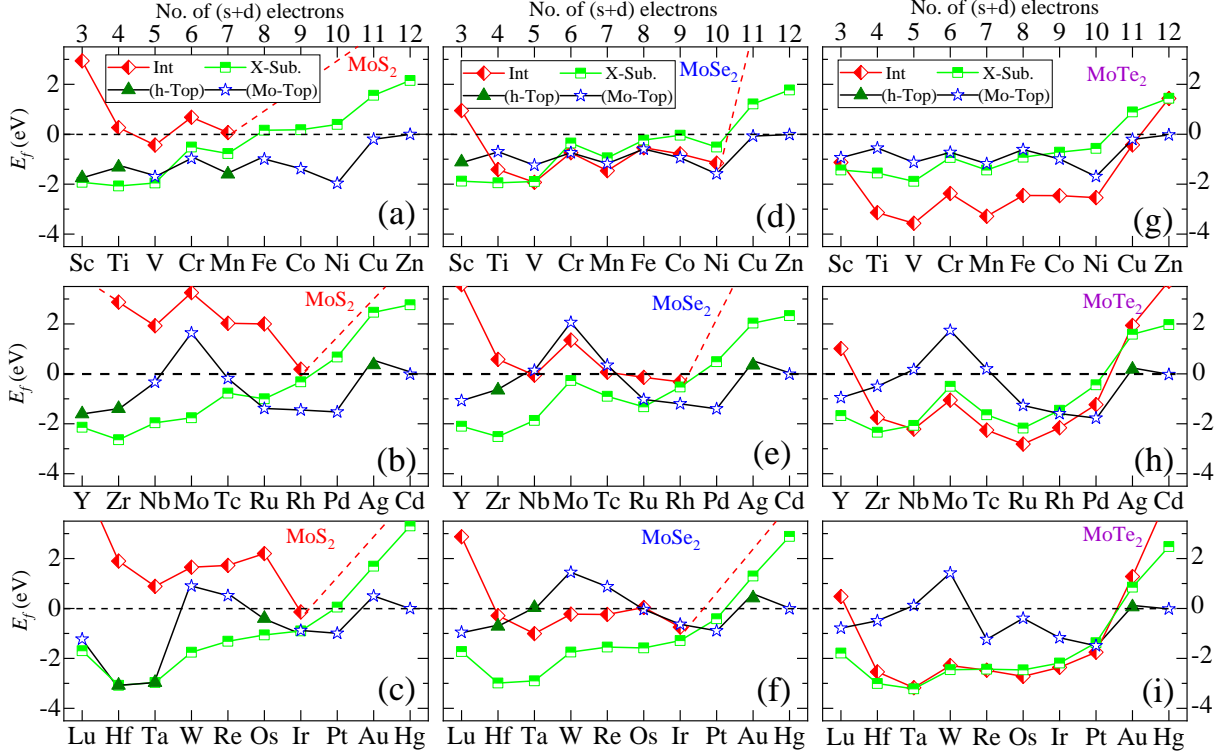
Figure 2: Formation energies of TM adatoms in the "h-Top" and "Mo-Top" positions on a (a-c) MoS$_2$, (d-f) MoSe$_2$ and (g-i) MoTe$_2$ layer, along with that of interstitial and substitutional chalcogen atom positions. Different symbols and colors are used to distinguish these atomic configurations. For adatoms, only the lowest-energy configurations are shown. Absence of the data points means that the configuration is either unstable or has much higher energy than other configurations, and in this case the trends are indicated by dashed lines.

nickel groups) are rather big and too inert to enter the lattice and remain on the surface. It is evident that the "Mo-Top" configuration is more stable than the "h-Top" for the majority of metals, especially in MoTe$_2$. The adatom energies are similar across different MoDCs, since the local neighborhood of the TM adatom remains similar and unaffected by the host lattice constant or bond lengths. The formation energies are mostly negative, meaning that two adatoms are more stable than isolated dimer, the notable exceptions being Mo and W. E_f for the "X-sub" configuration is also fairly similar across different MoDCs, as the TM atom is only bonded to three Mo atoms below and one chalcogen atom above it.

We also studied the stability of TM atoms in the "X-Sub" configuration and compared its formation energy to the energy of TM in the substitutional ("TM@X" configuration,

Fig. S2) calculated as a function of chalcogen Chem. potential μ_X, as this configuration is non-stoichiometric. The dependence of E_f on μ_X for Cr, Mo and W are presented in Fig. S3. It is evident that in the chalcogen-rich limit, the "X-Sub" configuration is energetically favorable. However, in the Mo-rich limit (when, e.g., many chalcogen vacancies are present), the "TM@X" configurations will mostly dominate, as X atoms will diffuse away from the TM and fill the vacancies. The results for all TMs in the TM- and X-rich limits are shown in Fig. S4. As the X-rich limit corresponds to the experimental conditions during the post-growth atom deposition, and because "X-Sub" configuration is lower in energy than "TM@X", we do not consider the latter configurations in this work.

The behavior of TM atoms on $MoTe_2$ is drastically different. For all TMs with a few exceptions, the interstitial configuration is energetically preferable, indicating that the deposited TMs can be incorporated into the sheets, in agreement with the available experimental data.[23,24] Such a behavior is related to the lengths of the primitive cell vectors of MoDCs, which are $3.18/3.32/3.55$ Å for $MoS_2/MoSe_2/MoTe_2$ respectively, and correspondingly to the amount of "free space" available for the interstitial atom. This is also evident from the pronounced lowering of the formation energies when moving from MoS_2 to $MoSe_2$ and further to $MoTe_2$. The trend of E_f is explained by the size of TM atoms and the Chem. potential of TM in dimers, see Fig. S10. The radius is the smallest near the middle of every row. Thus, the E_f is lower for the elements in the middle of the row; however a small hump at Cr group is due to the very low Chem. potential of corresponding TM atoms in the dimer.

In $MoTe_2$, interstitials are found to be the lowest energy configurations for most of the $3d$ TM (Ti-Cu) atoms. Only for Cu the energy difference is small (0.22 eV). For the $4d$ metals, the "X-Sub" configurations are competing with the "Int" configurations. The energy difference between the "Int" and "X-Sub" is negligibly small for $5d$ metals, except for Os and Pt atoms, which have a difference of $\approx$0.3 eV. Also, it is possible that in reality the chalcogen atom residing on top of the substituting TM atom will either desorb or diffuse out, leaving behind a TM impurity at the chalcogen site. While such defects are very likely
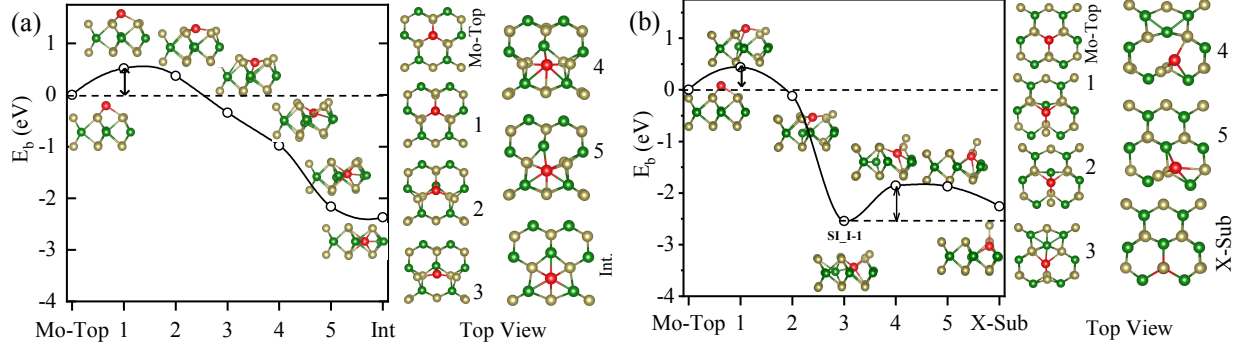
Figure 3: (a) Migration path and the associated energy between the "Mo-Top" and interstitial sites calculated for Nb atom in MoTe$_2$. (b) The same but for the "X-Sub" configuration. It is evident that both configurations are possible, although there is an additional potential barrier for the TM atom to take the substitutional position. Side views of the intermediate structures are shown as insets and the top views are shown along the side.

when chalcogen vacancies are already present in the sample, our results suggest that this can also occur in some cases for pristine MoDCs.

We stress that the actual behavior of the system during the deposition of metal atoms will depend on not only the energetics of the configurations, but also potential barriers separating different configurations, temperature and deposition rate. As an example, we calculated the barrier for the migration of several TM atoms from the "Mo-Top" to the "Int" and "X-Sub" configurations, as shown in Fig.3 for Nb. The energy is maximal when a TM atom is close to the Te plane. The Te atoms moves slightly outward to allow the migration of TM atom. The calculated barrier values are 0.78 eV, 0.5 eV, and 0.25 eV for V, Nb and Ta, respectively. These values indicate that diffusion is possible at moderate temperatures about 100°C. V, Nb and Ta TMs are chosen because they have lowest E_f in the respective series. The migration into the "X-Sub" configuration requires overcoming additional energy barrier, so that one can expect that when energies of these configurations are similar, incorporation of the TM atom as an interstitial is more likely.

Moreover, as evident from Fig. 3(b) other interstitial-type configurations are possible in MoTe$_2$ layer. It was previously found[23] that in MoTe$_2$ the interstitial Mo can easily move to the host lattice site and concurrently displace the atom neighboring to the interstitial
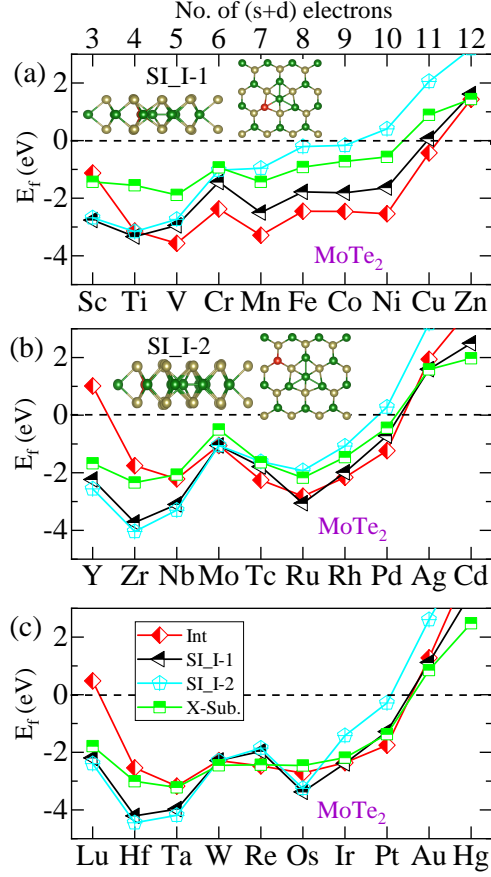
Figure 4: Formation energies of (a) $3d$, (b) $4d$ and (c) $5d$ TM substitutional impurities and interstitials in $MoTe_2$. The atomic configurations when a TM atom substitutes for a Mo atom, and a Mo interstitial is present are denoted as "SI". The representative atomic models are shown in the insets. The green, ochre-green, red colour balls represent host Mo, Te, and TM atoms, respectively.

site. Similarly, we expect that the TM interstitials can move to substitute Mo atom and displace Mo to the first ("SI_I-2") or second ("SI_I-1") nearest interstitial voids in the layers, see insets in Fig. 4. E_f of these two atomic configurations is also presented in Fig. 4, along with the energies of the Int and "X-Sub" configurations. It is evident that for $4d$ and $5d$ elements, these configurations are either lower in energy or competitive to the interstitial configuration, and thus we expect that they can be realized in the experiments. For $3d$ elements, Sc and Ti might substitute for Mo, but others are expected to mostly be
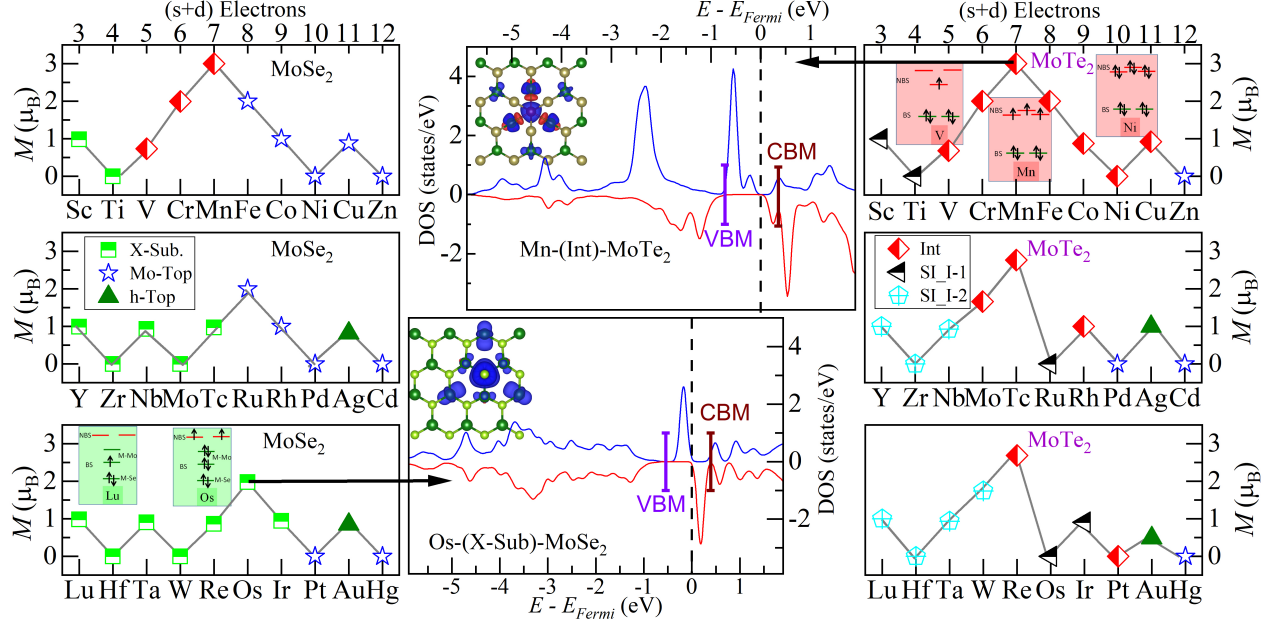
Figure 5: Magnetic moments (M) and electronic structure of MoSe$_2$ and MoTe$_2$ layers with TMs. Panels on the left/right show M of the lowest energy configurations of TM atoms in MoSe$_2$/MoTe$_2$ layers, respectively. The middle panels show the d-orbital splitting and spin polarization density distribution for interstitial Mn in MoTe$_2$ layer (top) and "X-Sub" Os in MoSe$_2$ layer (bottom), as they have highest magnetic moment in the series. The green, ochre-green, yellow-green, and red colour balls represent host Mo, Te, Se and TM atoms. The black and red colours show up and down spin states of the d orbitals and the position of Fermi level is indicated by the dotted line. The top-right panel presents a schematic of the d orbital splitting for interstitial TM atoms and the bottom-left panel shows a schematic of d orbital splitting for the "X-Sub" configuration.

in the interstitial configuration. At the same time, the Mo-substitutional configurations are unlikely in MoSe$_2$ (Fig. S5) and MoS$_2$ due to considerably lower energies of the "X-Sub" or interstitial configurations, respectively.

We further studied the electronic and magnetic properties of TM-doped MoDCs. All configurations give rise to new states localized at or near the impurity atoms, see Fig. 5 and also Figs. S6-S9, and some of them exhibit magnetic moments M. The plots of M against the number of $(s + d)$ electrons, Fig. 5, show that for interstitial $3d$ atoms, M increases up to the maximum value of 3 μ_B in the middle of the row (e.g., for Mn), then decreases again. Since the interstitial site is stable for many TM atoms, at least $3d$ atoms in MoTe$_2$, we analyzed the density of states of interstitial TM atoms in MoTe$_2$ layer as

shown in Figs. 5 and S6. The data indicates that filling of the d orbitals is responsible for the magnetic moments of TM atoms in interstitial sites of MoDC layers. The d orbitals of interstitial TM atom impurities can be split into two groups as shown in the schematic in Figs. 5. There are doubly degenerate bonding states which are the lowest in energy and formed by the hybridization of surrounding Mo-4d orbitals and the d orbitals of the TM atom. The first TM atom in every series possesses three valence electrons involved in bonding with the surrounding Mo atoms. For example, in MoTe$_2$, the doubly degenerate bonding states are partially filled by three electrons, resulting in 1 μ_B. When the TM has four electrons, the bonding states are completely filled for Ti, Zr, and Hf, which increases the electronic stability (cf. Fig. 2). After filling bonding orbitals, electrons occupy the non-bonded d orbitals. Thus, M increases step-wise from V to Mn, then it decreases due to the pairing of electrons. It is interesting to note that overall similar trends have been reported for TM substitutional impurities in graphene.[40,41] Similarly, Co substitutional impurity in WS$_2$ layer has 3 μ_B magnetic moment and biggest spin gap among the 3d TM atoms.[42] For Ni, all the electrons are paired in non-bonded states to result in zero magnetic moment. For Cu atom, the anti-bonding state is filled to give 1 μ_B.

On the other hand, the trend of magnetic moments for 4d and 5d elements in MoSe$_2$ layer is different, as they are mostly stable in the "X-Sub" configuration. To understand the d orbital filling, we studied the electronic structure of all 5d metals in MoSe$_2$ layer in more detail. The density of states and spin density for all 5d elements are shown in Figs S8 and S9. In the "X-Sub" configuration, the d orbitals are split into three groups as shown in the schematic in Figs. 5; (i) TM-Se bonding state, (ii)two TM-Mo bonding states and (iii) doubly degenerated non-bonded states. Among these, the TM-Se bonding state has the lowest energy for any TM atom. For Lu, TM-Se fills the TM-Mo bonding states, which results in $M = 1\mu_B$. Successively, the second TM-Mo bonding state and doubly degenerated non-bonded states are filled by the ($s + d$) electrons. Thus, all the bonding states are filled for W atom. Although this and the interstitial configuration with four ($s + d$) electrons (e.g.

Ti) have all the bonding states filled, the W "X-Sub" configuration exhibits high formation energy. As said earlier, this is due to very low Chem. potential of W. Interestingly, a high magnetic moment is observed for Os atom, due to half filled doubly degenerated non-bonded states.

As compared to the traditional introduction of dopants/impurities during growth or ion implantation, the post-synthesis doping/materials modifications discussed in this work and demonstrated previously in the experiments[23,24] has several advantages. It enables local patterning or formation of metastable configurations that cannot be realized during high-growth temperature synthesis, especially in MoTe$_2$, where the incorporation of TM atoms into the crystal framework can energetically be favorable over adatom clustering. Thus to achieve impurity doping at interstitial sites experimentally, simple vapor deposition of TM atoms in vacuum onto the 2D sheet should be sufficient. Vapor deposition is a soft process with no secondary damage by high-energy ion beams used in implantation processes. On the other hand, we note that only in the dilute limit single atom defects will form and depending on their mobility and concentration complex defect structures like the observed MTBs may appear.[43] In addition to introducing magnetism into 2D materials by the impurities discussed here, dispersed TM atoms may add also other functionalities, such as being Chem.ly active sites for single atom catalysis or single photon emission.[44,45] We also note that incorporation of metals into the semiconductor during vapor deposition may affect the contact formation. Defect states induced in the 2D materials by the impurities will pin the Fermi-level at the neutrality point of these defect states, and thus no Schottky-contact can form.[46] Finally, our findings can also be useful for understanding the operating principles of 2D memristors, where one of the suggested mechanism involves formation of conducting filaments via diffusion of metal atoms from the contacts.[47]

In summary, using DFT calculations, we studied the energetics of *all* TM adatoms and interstitials in MoDCs and showed that the incorporation of TMs into the atomic network is possible instead of trivial clustering of TMs on the surface, especially in MoTe$_2$, which has

the largest spacing between the host atoms. We further demonstrated that many impurity configurations possess localized magnetic moments. By analyzing the trends in energetics and value of magnetic moments across the periodic table, we rationalized the results through the value of TM atomic radii and the number of $(s + d)$ electrons available for bonding, and suggest most promising TMs for adding magnetism in MoDCs. Our results are in line with the available experimental data and should further guide the experimental effort aimed at adding magnetism and other new functionalities to 2D material by a rather simple post-synthesis TM atom deposition technique.

Acknowledgement

Supporting information

The Supporting Information is available free of charge on the ACS Publications website at DOI: 10.1021/xxxxxxxxxxxxxx. Atomic structures of symmetric/distorted "X-sub" configurations, along with the "TM@X" configuration are illustrated. Formation energies and magnetic moment for different atomic structures of TM atoms deposited on MoS_X layers are presented. Spin-polarization densities are shown, as obtained from first-principles calculations.

References

(1) Nastasi, M.; Mayer, J.; Hirvonen, J. *Ion-Solid Interactions - Fundamentals and Applications*; Cambridge University Press: Cambridge, UK, 1996.

(2) Yu, P.; Cardona, M. *Fundamentals of Semiconductors*; Springer, 2010.

(3) Wu, Z.-S.; Winter, A.; Chen, L.; Sun, Y.; Turchanin, A.; Feng, X.; Mullen, K. Three-Dimensional Nitrogen and Boron Co-doped Graphene for High-Performance All-Solid-State Supercapacitors. *Adv. Mater.* **2012**, *24*, 5130–5135.

(4) Zhao, L.; Levendorf, M.; Goncher, S.; Schiros, T.; Pálová, L.; Zabet-Khosousi, A.; Rim, K. T.; Gutiérrez, C.; Nordlund, D.; Jaye, C.; Hybertsen, M.; Reichman, D.; Flynn, G. W.; Park, J.; Pasupathy, A. N. Local atomic and electronic structure of boron Chem. doping in monolayer graphene. *Nano Lett.* **2013**, *13*, 4659–65.

(5) Ramasse, Q.; Seabourne, C. R.; Kepaptsoglou, D.-M.; Zan, R.; Bangert, U.; Scott, A. J. Probing the bonding and electronic structure of single atom dopants in graphene with electron energy loss spectroscopy. *Nano Lett.* **2013**, *13*, 4989–95.

(6) Tripathi, M.; Markevich, A.; Böttger, R.; Facsko, S.; Besley, E.; Kotakoski, J.; Susi, T. Implanting Germanium into Graphene. *ACS Nano* **2018**, *12*, 4641–4647.

(7) Zhao, W.; Höfert, O.; Gotterbarm, K.; Zhu, J.; Papp, C.; Steinrück, H.-P. Production of Nitrogen-Doped Graphene by Low-Energy Nitrogen Implantation. *J. Phys. Chem. C* **2012**, *116*, 5062–5066.

(8) Susi, T.; Hardcastle, T. P.; Hofsäss, H.; Mittelberger, A.; Pennycook, T. J.; Mangler, C.; Drummond-Brydson, R.; Scott, A. J.; Meyer, J. C.; Kotakoski, J. Single-atom spectroscopy of phosphorus dopants implanted into graphene. *2D Mater.* **2017**, *4*, 021013.

(9) Bangert, U.; Pierce, W.; Kepaptsoglou, D. M.; Ramasse, Q.; Zan, R.; Gass, M. H.; Van den Berg, J. a.; Boothroyd, C. B.; Amani, J.; Hofsäss, H. Ion Implantation of Graphene-Toward IC Compatible Technologies. *Nano Lett.* **2013**, *13*, 4902–4907.

(10) Wang, Q. H.; Kalantar-Zadeh, K.; Kis, A.; Coleman, J. N.; Strano, M. S. Electron-

ics and Optoelectronics of Two-Dimensional Transition Metal Dichalcogenides. *Nat. Nanotech.* **2012**, *7*, 699–712.

(11) Chhowalla, M.; Shin, H. S.; Eda, G.; Li, L.-J.; Loh, K. P.; Zhang, H. The Chemistry of Two-Dimensional Layered Transition Metal Dichalcogenide nanosheets. *Nat. Chem.* **2013**, *5*, 263–275.

(12) Miro, P.; Audiffred, M.; Heine, T. An atlas of two-dimensional materials. *Chem. Soc. Rev.* **2014**, *43*, 6537–6554.

(13) Liu, G.-B.; Xiao, D.; Yao, Y.; Xu, X.; Yao, W. Electronic structures and theoretical modelling of two-dimensional group-VIB transition metal dichalcogenides. *Chem. Soc. Rev.* **2015**, *44*, 2643–2663.

(14) Lin, Y.-C.; Dumcenco, D. O.; Komsa, H.-P.; Niimi, Y.; Krasheninnikov, A. V.; Huang, Y.-S.; Suenaga, K. Properties of individual dopant atoms in single-layer MoS2: atomic structure, migration, and enhanced reactivity. *Adv. Mater.* **2014**, *26*, 2857–61.

(15) Wang, S.; Robertson, A.; Warner, J. H. Atomic structure of defects and dopants in 2D layered transition metal dichalcogenides. *Chem. Soc. Rev.* **2018**, *47*, 6764–6794.

(16) Lin, Y. C.; Li, S.; Komsa, H.-P.; Chang, L. J.; Krasheninnikov, A. V.; Eda, G.; Suenaga, K. Revealing the Atomic Defects of WS2 Governing Its Distinct Optical Emissions. *Adv. Func. Mater.* **2017**, *28*, 1704210.

(17) Gao, J.; Kim, Y. D.; Liang, L.; Idrobo, J. C.; Chow, P.; Tan, J.; Li, B.; Li, L.; Sumpter, B. G.; Lu, T. M.; Meunier, V.; Hone, J.; Koratkar, N. Transition-Metal Substitution Doping in Synthetic Atomically Thin Semiconductors. *Adv. Mater.* **2016**, *28*, 9735–9743.

(18) Li, Z.; Chen, F. Ion beam modification of two-dimensional materials: Characterization, properties, and applications. *Appl. Phys. Rev.* **2017**, *4*, 011103.
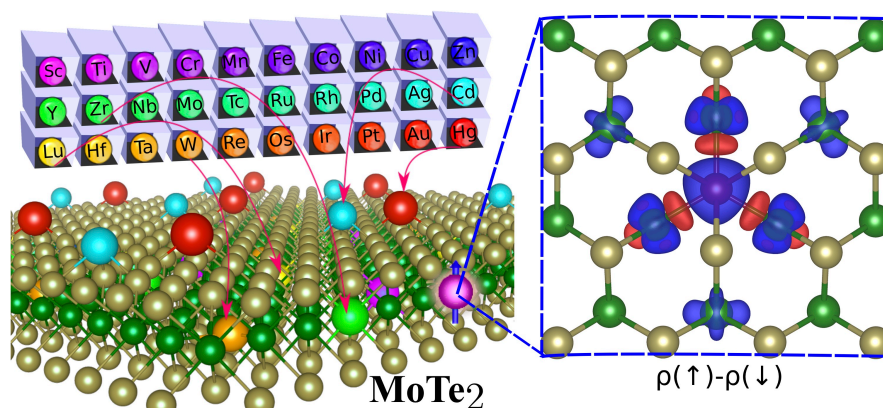
(19) Lin, Z.; Carvalho, B. R.; Kahn, E.; Lv, R.; Rao, R.; Terrones, H.; Pimenta, M. A.; Terrones, M. Defect Engineering of Two-Dimensional Transition Metal Dichalcogenides. *2D Mater.* **2016**, *3*, 022002.

(20) Nguyen, L.; Komsa, H.-P.; Khestanova, E.; Kashtiban, R. J.; Peters, J. J. P.; Lawlor, S.; Sanchez, A. M.; Sloan, J.; Gorbachev, R. V.; Grigorieva, I. V.; Krasheninnikov, A. V.; Haigh, S. J. Atomic Defects and Doping of Monolayer NbSe2. *ACS Nano* **2017**, *11*, 2894–2904.

(21) Lu, A.-Y.; Zhu, H.; Xiao, J.; Chuu, C.-P.; Han, Y.; Chiu, M.-H.; Cheng, C.-C.; Yang, C.-W.; Wei, K.-H.; Yang, Y.; Wang, Y.; Sokaras, D.; Nordlund, D.; Yang, P.; Muller, D. A.; Chou, M.-Y.; Zhang, X.; Li, L.-J. Janus monolayers of transition metal dichalcogenides. *Nat. Nanotech.* **2017**, *12*, 744–749.

(22) Ma, Q.; Isarraraz, M.; Wang, C. S.; Preciado, E.; Klee, V.; Bobek, S.; Yamaguchi, K.; Li, E.; Odenthal, P. M.; Nguyen, A.; Barroso, D.; Sun, D.; von Son Palacio, G.; Gomez, M.; Nguyen, A.; Le, D.; Pawin, G.; Mann, J.; Heinz, T. F.; Rahman, T. S.; Bartels, L. Postgrowth Tuning of the Bandgap of Single-Layer Molybdenum Disulfide Films by Sulfur/Selenium Exchange. *ACS Nano* **2014**, *8*, 4672–4677.

(23) Coelho, P. M.; Komsa, H.-P.; Coy Diaz, H.; Ma, Y.; Krasheninnikov, A. V.; Batzill, M. Post-Synthesis Modifications of Two-Dimensional MoSe2 or MoTe2 by Incorporation of Excess Metal Atoms into the Crystal Structure. *ACS Nano* **2018**, *12*, 3975–3984.

(24) Coelho, P. M.; Komsa, H.-P.; Lasek, K.; Kalappattil, V.; Karthikeyan, J.; Phan, Y., Manh-Huong; Krasheninnikov, A. V.; Batzill, M. Room temperature ferromagnetism in MoTe2 by post-growth incorporation of vanadium impurities. *Adv. El. Mater.* **2019**, *5*, 1900044.

(25) Wang, J.; Sun, F.; Yang, S.; Li, Y.; Zhao, C.; Xu, M.; Zhang, Y.; Zeng, H. Robust ferromagnetism in Mn-doped MoS2 nanostructures. *Appl. Phys. Lett.* **2016**, *109*, 092401.

(26) Wang, D.; Li, X. B.; Han, D.; Tian, W. Q.; Sun, H. B. Engineering two-dimensional electronics by semiconductor defects. *Nano Today* **2017**, *16*, 30–45.

(27) Dolui, K.; Rungger, I.; Das Pemmaraju, C.; Sanvito, S. Possible doping strategies for MoS_2 monolayers: An ab initio study. *Phys. Rev. B: Condens. Matter Mater. Phys.* **2013**, *88*, 075420.

(28) Laskar, M. R.; Nath, D. N.; Ma, L.; Lee, E. W.; Lee, C. H.; Kent, T.; Yang, Z.; Mishra, R.; Roldan, M. A.; Idrobo, J.-C.; Pantelides, S. T.; Pennycook, S. J.; Myers, R. C.; Wu, Y.; Rajan, S. p-type doping of MoS2 thin films using Nb. *Appl. Phys. Lett.* **2014**, *104*, 092104.

(29) Lu, S.-C.; Leburton, J.-p. Electronic structures of defects and magnetic impurities in MoS2 monolayers. *Nanoscale Res. Lett.* **2014**, *9*, 676.

(30) Onofrio, N.; Guzman, D.; Strachan, A. Novel doping alternatives for single-layer transition metal dichalcogenides. *J. Appl. Phys.* **2017**, *122*, 185102.

(31) Andriotis, A. N.; Menon, M. Tunable magnetic properties of transition metal doped MoS_2. *Phys. Rev. B: Condens. Matter Mater. Phys.* **2014**, *90*, 125304.

(32) Ataca, C.; Ciraci, S. Functionalization of Single-Layer MoS_2 Honeycomb Structures. *J. Phys. Chem. C* **2011**, *115*, 13303–13311.

(33) Rastogi, P.; Kumar, S.; Bhowmick, S.; Agarwal, A.; Chauhan, Y. S. Doping Strategies for Monolayer MoS2 via Surface Adsorption: A Systematic Study. *J. Phys. Chem. C* **2014**, *118*, 30309–30314.

(34) Saab, M.; Raybaud, P. Tuning the Magnetic Properties of MoS2 Single Nanolayers by 3d Metals Edge Doping. *J. Phys. Chem. C* **2016**, *120*, 10691–10697.

(35) Kresse, G.; Furthmüller, J. Efficiency of ab-initio total energy calculations for metals and semiconductors using a plane-wave basis set. *Comp. Mater. Sci.* **1996**, *6*, 15.

(36) Kresse, G.; Furthmüller, J. Efficient iterative schemes for ab initio total-energy calculations using a plane-wave basis set. *Phys. Rev. B: Condens. Matter Mater. Phys.* **1996**, *54*, 11169–11186.

(37) Perdew, J. P.; Burke, K.; Ernzerhof, M. Generalized Gradient Approximation Made Simple. *Phys. Rev. Lett.* **1996**, *77*, 3865–3868.

(38) Zhu, Y.; Ramasse, Q. M.; Brorson, M.; Moses, P. G.; Hansen, L. P.; Kisielowski, C. F.; Helveg, S. Visualizing the Stoichiometry of Industrial-Style Co-Mo-S Catalysts with Single-Atom Sensitivity. *Angew. Chem. Int. Ed.* **2014**, *53*, 10723–10727.

(39) Zhang, K.; Feng, S.; Wang, J.; Azcatl, A.; Lu, N.; Addou, R.; Wang, N.; Zhou, C.; Lerach, J.; Bojan, V.; Kim, M. J.; Chen, L.-Q.; Wallace, R. M.; Terrones, M.; Zhu, J.; Robinson, J. A. Manganese Doping of Monolayer MoS2: The Substrate Is Critical. *Nano Lett.* **2015**, *15*, 6586–6591.

(40) Krasheninnikov, A. V.; Lehtinen, P. O.; Foster, A. S.; Pyykkö, P.; Nieminen, R. M. Embedding Transition-Metal Atoms in Graphene: Structure, Bonding, and Magnetism. *Phys. Rev. Lett.* **2009**, *102*, 126807.

(41) Santos, E. J. G.; Ayuela, A.; Sánchez-Portal, D. First-principles study of substitutional metal impurities in graphene: structural, electronic and magnetic properties. *New J. Phys.* **2010**, *12*, 053012.

(42) Hyun, J.; Kim, M. Electronic and Magnetic Properties of Transition-Metal-Doped WS2 Monolayer; First-Principles Investigations. *IEEE Trans. Magn.* **2019**, *55*, 7000204.

(43) Batzill, M. Mirror twin grain boundaries in molybdenum dichalcogenides. *J. Phys.: Condens. Matter* **2018**, *30*, 493001.

(44) Hong, J.; Jin, C.; Yuan, J.; Zhang, Z. Atomic Defects in Two-Dimensional Materi-

als: From Single-Atom Spectroscopy to Functionalities in Opto-/Electronics, Nano-magnetism, and Catalysis. *Adv. Mater.* **2017**, *29*, 1606434.

(45) Gupta, S.; Yang, J.-H.; Yakobson, B. I. Two-Level Quantum Systems in Two-Dimensional Materials for Single Photon Emission. *Nano Lett.* **2019**, *19*, 408–414.

(46) Liu, Y.; Guo, J.; Zhu, E.; Liao, L.; Lee, S.-j.; Ding, M.; Shakir, I.; Gambin, V.; Huang, Y.; Duan, X. Approaching the Schottky-Mott limit in van der Waals metal-semiconductor junctions. *Nature* **2018**, *557*, 696–700.

(47) Xu, R.; Jang, H.; Lee, M.-H.; Amanov, D.; Cho, Y.; Kim, H.; Park, S.; Shin, H.-j.; Ham, D. Vertical MoS2 Double-Layer Memristor with ElectroChem. Metallization as an Atomic-Scale Synapse with Switching Thresholds Approaching 100 mV. *Nano Lett.* **2019**, *19*, 2411–2417.

TOC figure.